# Bi-level Energy Trading Model Incorporating Large-scale Biogas Plant and Demand Response Aggregator

Hanyu Yang, Canbing Li, Ruanming Huang, Feng Wang, Lili Hao, Qiuwei Wu, and Long Zhou

***Abstract*—Increasing intermittent renewable energy sources (RESs) intensifies the imbalance between demand and generation, entailing the diversification of the deployment of electrical energy storage systems (ESSs). A large-scale biogas plant (LBP) installed with heating devices and biogas energy storage (BES) usually exhibits a storage-like characteristic of accommodating an increasing penetration level of RES in rural areas, which is addressed in this paper. By utilizing the temperature-sensitive characteristic of anaerobic digestion that enables the LBP to exhibit a storage-like characteristic, this paper proposes a bi-level energy trading model incorporating LBP and demand response aggregator (DRA) simultaneously. In this model, social welfare is maximized at the upper level while the profit of DRA is maximized at the lower level. Compared with cases only with DRA, the results show that the proposed model with the LBP improves the on-site accommodation capacity of photovoltaic (PV) generation up to 6.3%, 18.1%, and 18.9% at 30%, 40%, and 50% PV penetration levels, respectively, with a better economic performance. This nonlinear bi-level problem is finally recast by a single-level mathematical program with equilibrium constraints (MPEC) using Karush-Kuhn-Tucker (KKT) conditions and solved by the Cplex solver. The effectiveness of the proposed model is validated using a 33-bus test system and a sensitivity analysis is provided for analyzing what parameter influences the accommodation capacity most.**

***Index Terms*—Biomass energy, renewable energy resource, energy trading, demand response, distribution system.**

Manuscript received: September 26, 2021; revised: December 27, 2021; accepted: March 22, 2022. Date of CrossCheck: March 22, 2022. Date of online publication: April 22, 2022.

This work was supported by the National Natural Science Foundation of China (No. 51977062).



H. Yang and L. Hao are with the College of Electrical Engineering and Control Science, Nanjing Tech University, Nanjing, China (e-mail: hyang73@outlook.com; lili_hao@163.com).

C. Li (corresponding author) is with the School of Electronic Information and Electrical Engineering, Shanghai Jiao Tong University, Shanghai 200240, China (e-mail: licanbing@sjtu.edu.cn).

R. Huang is with the Economic and Technological Research Institute of Shanghai Electric Power Company, Shanghai, China (e-mail: hrmjobhrms@163.com).

F. Wang is with the College of Electrical and Information Engineering, Hunan University, Changsha 410082, China (e-mail: 1643295433@qq.com).

Q. Wu is with Tsinghua-Berkeley Shenzhen Institute, Tsinghua Shenzhen International Graduate School, Tsinghua University, Shenzhen 518055, China (e-mail: quiwudtu@gmail.com).

L. Zhou is with the Information Center of Guangdong Power Grid Company Limited, Guangzhou 528000, China (e-mail: zhoulong20021013@163.com).

DOI: 10.35833/MPCE.2021.000632

## NOMENCLATURE

### A. Indices and Sets

| | |
|---|---|
| $\Pi_k$ | Set of buses connected to bus $k$ |
| $\Omega_k$ | Set of combined heat and power (CHP) unit $g$, substation $w$, photovoltaic (PV) farm $p$, and large-scale biogas plant (LBP) located at bus $k$ |
| $i$, $j$, $k$ | Indices of buses |
| $s$ | Index of breakpoints |
| $SK$, $SW$, $SP$ $SG$, $SA$, $SL$ | Sets of buses, substations, PV farms, CHP units, demand response aggregators (DRAs), lines |
| $SN$ | Set of the extreme points in the feasible operation region of CHP unit |
| $t$, $w$, $p$, $g$, $a$, $l$ | Indices of hour, substation, PV farm, LBP (CHP unit), DRA, line |

### B. Parameters

| | |
|---|---|
| $\alpha_{11}$, $\alpha_{12}$, $\alpha_{21}$, $\alpha_{22}$ | Coefficients observed by a series of full-scale experiments on predicting biogas yield |
| $\delta^{Agg}$ | Profit guarantee factor of DRA |
| $\eta_{con}$, $\eta_e$ | Conversion efficiencies of CHP unit and electric heating device |
| $\eta_{PQ}$ | Power factor of demand and CHP unit |
| $\eta^{loss}$ | Heat loss in the heat pipes |
| $\eta_{BES}$ | Inflating/deflating efficiency of biogas energy storage (BES) |
| $\varepsilon^{Dem}$ | Multiplier of load forecasting |
| $A_{air,AD}$, $V_{AD}$ | Surface area and volume of anaerobic digester (AD) |
| $B_0$, $S_0$ | Biochemical methane potential and the volatile solid concentration of influent feedstock |
| $c_{AD}$, $\rho_{AD}$ | Heat capacity and density of digesting manure |
| $C_t^{RT}$, $C_t^{DA}$ | Prices of procuring electricity from the main grid in the real-time and day-ahead markets |
| $C^{PV}$, $C^{CHP}$ | Generation costs of PV and CHP unit |
| $C^D$, $C_{loss}$ | Prices of electricity sold to customers and network losses |
| $C_{at}^{Aggpro}$ | Contractual price signed between customers and DRA |

$dr^{\max}$ The maximum capacity of demand response (DR)

$\bar{G}^{CHP}$ The maximum biogas consumption rate of CHP unit

$\bar{G}^{BES}, \underline{G}^{BES}$ The maximum and minimum volumes of BES

$HRT$ Hydraulic retention time

$P^{ramp}, H^{ramp}$ The maximum power and heat ramping rates of CHP unit

$I_{\max}, I_{\min}$ Upper and lower limits of squared magnitude of current

$K^{dis}$ Conductivity coefficient of surfaces of AD

$K$ Dimensionless kinetic parameter

$m_{bio}$ Hourly mass flow of the influent feedstock

$P_{\max}^{grid}$ The maximum power from the distribution system to the LBP

$\bar{P}_{kt}^{Dem}$ Predictive active power demand at bus $k$

$\bar{P}_{at}^{Agg}, \underline{P}_{at}^{Agg}$ Upper and lower limits of active power aggregated at DRA

$\bar{P}_{pt}^{PV}$ Forecasted power generation of PV farm

$\bar{Q}_{at}^{Agg}, \underline{Q}_{at}^{Agg}$ Upper and lower limits of reactive power aggregated at DRA $a$

$R_{ij}, X_{ij}, Z_{ij}$ Resistance, reactance, and impedance of line $l$ from bus $i$ to bus $j$

$S_{w,\max}$ The maximum capacity of substation $w$

$S$ Total number of breakpoints

$T_t^{air}$ Ambient temperature

$V_i^{\max}, V_i^{\min}$ Upper and lower limits of squared magnitude of pressure at bus $i$

### C. Variables

$\mu_t$ The maximum specific daily growth rate of micro-organisms for mesophilic digestion

$C_{at}^{Agg}$ Power purchase price from DRA

$dr_{kt}$ DR capacity at bus $k$

$G_t, G_t^{BES}$ Hourly biogas yield and volume of biogas in BES

$G_t^{CHP}$ Biogas consumption rate of CHP unit

$H_t^{dis}, H_t^{heat}$ Dissipating heat of AD and heat required for warming influent feedstock

$H_t^{AD}$ Total heat injected into AD

$H_t^{grid}$ Heat produced by the electric heating device

$m_t$ Binary variable indicating the startup/shutdown status of CHP unit

$P_{kt}^{D}, Q_{kt}^{D}$ Real-time active and reactive power loads at bus $k$

$P_{ijt}, Q_{ijt}$ Active and reactive power flows from bus $i$ to bus $j$

$P_{kt}^{Dem}$ Active power demand at bus $k$

$P_t^{grid}$ Active power from the distribution system to AD for electric heating

$P_t^{CHP}, Q_t^{CHP}$ Active power, reactive power, and heat power generated by CHP unit

$H_t^{CHP}$

$P_{wt}^{DA}, Q_{wt}^{DA}$ Day-ahead active and reactive power purchased from the main grid

$P_{pt}^{PV}$ Actual generation of PV farm

$P_{wt}^{RT}, Q_{wt}^{RT}$ Active and reactive power exchanged with the main grid in the real-time market

$P_{wt}^{DA}, Q_{wt}^{DA}$ Active and reactive power exchanged with the main grid in the day-ahead market

$P_{wt}^{Sub}, Q_{wt}^{Sub}$ Active and reactive power from substation $w$

$P_{at}^{Agg}, Q_{at}^{Agg}$ Active and reactive power aggregated by DRA

$R^{RES}, R^{Agg}$ Power generation costs of RES and DRA

$R^{RT}, R^{DA}$ Costs of purchasing power in real-time and day-ahead markets

$R^{loss}, dr_{kt}$ Network losses and DR capacity

$R^{D}$ Total benefit of customers

$T_t$ Digesting temperature

$T_s$ Intervals over the range of digesting temperature

$V_{it}, I_{ijt}$ Squared voltage at bus $i$ and current flow between bus $i$ and bus $j$

$y_{tn}$ Auxiliary variable indicating operation of CHP unit

$z_{ts}, q_{ts}$ Auxiliary variables for piecewise linearization

## I. Introduction

RAPID proliferation of intermittent renewable energy sources (RESs) intensifies the imbalance between the generation and demand, which urges a further diversification and deployment of the electrical energy storage system (ESS) [1], [2]. The existing ESSs implemented in the power system to offset the deviations between demand and generation caused by RESs can be divided into three types: mechanical ESS (e. g., pumped-storage power plants, flywheel ESS, compressed air ESS), chemical ESS (e. g., hydrogen storage), and electrochemical ESS, especially batteries [3], [4].

Numerous researches have been conducted on those above-mentioned ESSs that participate in the energy market for providing system-level grid-support service to maintain the power balance while accommodating a high penetration level of RESs [5]. Among multiple ESSs, mechanical ESSs that take advantage of kinetic and gravitational forces to store inputted energy is one of the large-scale ESS technologies and the most mature one. The modeling of the pumped-storage power plant [6]-[9], flywheel ESS [10], and compressed air ESS [11], [12] incorporating their respective physical boundary conditions and characteristics as well as their commercialized application in the energy market has been explored by many scholars. With respect to chemical ESSs, the hydrogen plant has been demonstrated as a promising massive ESS by converting power to hydrogen and methane through electrolyzation. A bi-level comprehensive strategic bidding model of a profit-driven hydrogen plant acting as price-maker within electricity, natural gas, and carbon emission permit markets is proposed in [13]. As opposed to the mechanical

and chemical ESSs which are usually applied in the bulk power system, batteries representative of the electrochemical ESSs that have a shorter response time and are more flexible in site selection are more applicable in the distribution system [14]-[16]. In [15], a two-stage coordinated approach of price-based batteries is proposed to minimize the total operating cost and enhance operational violations caused by the RES uncertainty. In [16], a systematic assessment is proposed to evaluate the flexibility level of a power system integrating demand response aggregators (DRAs) and batteries to accommodate RES considering fast ramping units.

With the promotion of distributed PV in the rural revitalization in China, the requirement of ESSs will no longer constrain to the bulk power system or city center but also extend to the rural areas. However, considering that a wide popularization of batteries in rural areas is still in a long run, making use of the on-site resources to deal with the increasing penetration level of RESs becomes a necessity.

Accordingly, we investigated the above-mentioned ESSs. It is their characteristics of converting, storing, and discharging one energy to another energy that makes themselves have the potential to mitigate the intermittent of RESs. Following this basic characteristic, we observed that the anaerobic digestion process of large-scale biogas plant (LBP) that is widely deployed in rural areas is similar to the electrolyzation of hydrogen plants. Due to the temperature-sensitive anaerobic digestion, LBP can utilize electricity for maintaining the digesting temperature and enhancing the biogas yield. Then, the surplus biogas can be served as a backup fuel in the biogas energy storage (BES) supplying electricity when the electricity supply is short, and finally, a circular conversion of power-biogas-power is formulated [17]. This storage-like shift is characterized by its temperature-sensitive anaerobic digestion, i.e., the biogas yield increases with temperature, which surprisingly enables the LBP a promising potential in providing more capacity for accommodating the increasing penetration level of RESs and balancing the power supply in rural areas [18].

In fact, integrating anaerobic digester (AD) with thermal technologies, e.g., wind energy [19], solar energy [20], [21], geothermal energy [22], etc., for maintaining the temperature or increasing the biogas yield during the anaerobic digestion has been studied, which are sometimes termed as the complementarity between multiple energies and biogas in [21]. However, the existing studies on complementarity are inclined to modeling or analyzing the thermodynamics of the anaerobic digestion at a microscopic level, neglecting the applications of its storage-like characteristic for accommodating a high penetration level of RESs from a macroscopic level [19]-[22]. Thus, in this paper, as an extension of our previous work that utilized the complementarity of biogas and solar energy for planning an energy hub [23], we further quantify the storage-like characteristic of LBP for accommodating RES and apply it in an energy trading model. The contributions are summarized as follows.

1) The conversion process of power-biogas-power consisting of biogas generation, storage, and consumption that makes LBP exhibit a storage-like characteristic for better accommodating RESs is addressed in this paper.

2) The storage-like characteristic of LBPs is firstly applied in the energy market. Considering that LBP and DRA can both provide capacity for accommodating the on-site use of RESs, a bi-level energy trading model is proposed for quantifying the accommodation capacity contributed by LBPs, where the social welfare and the profit of DRAs are both maximized.

The remainder of this paper is organized as follows. Section II introduces the storage-like characteristic of LBPs. Section III presents the mathematical formulations of the proposed bi-level energy trading model. In Section IV, the solution method of this problem is presented. Section V illustrates the case studies and Section VI draws the conclusions.

## II. Storage-like Characteristic of LBPs

In this section, the model of the storage-like characteristic of LBPs is presented, whose operation schematic diagram is illustrated in Fig. 1. The LBP consists of AD, BES, and combined heat and power (CHP) unit. The LBP can be used to provide capacity for accommodating the on-site use of RESs by the following three steps: biogas generation, storage and consumption, and formulation of the storage-like inflating/deflating in the BES.

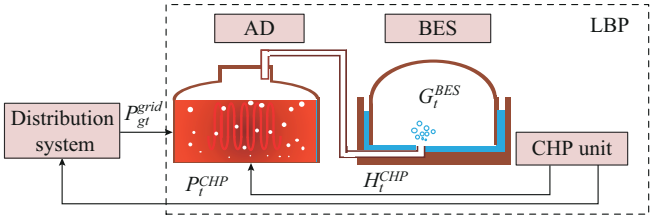


Fig. 1. Operation schematic diagram for model of storage-like characteristic of LBPs.

In the step of biogas generation in Fig. 1, constraints (1) and (2) describe that the total heating power for AD comes from the CHP unit and electric heating devices driven by the power from the distribution system. Usually, the optimal digestion temperature of mesophilic digestion is within 20-45 °C. It is much higher than the ambient temperature, especially in winter. Thus, the thermal energy required in the AD usually consists of two parts: one is for heating the continuous influent feedstock whose temperature equals the ambient temperature up to the digesting temperature; the other is for maintaining temperature to offset the heat dissipation from the AD to the surroundings through surfaces like cover and walls [21], which is calculated in constraints (3) and (4). Correspondingly, the thermal equilibrium with digesting temperature evolution based on the energy conservation rules is given in constraint (5).

$$H_t^{AD} = H_t^{grid} + \eta^{loss} H_t^{CHP} \quad \forall t \tag{1}$$

$$H_t^{grid} = \eta_e P_t^{grid} \quad \forall t \tag{2}$$

$$H_t^{dis} = K^{dis} A_{air,AD} \left( T_t - T_t^{air} \right) \quad \forall t \tag{3}$$

$$H_t^{heat} = c_{AD} m_{bio} \left( T_t - T_t^{air} \right) \quad \forall t \tag{4}$$

$$T_{t+1}=T_t+\frac{H_t^{grid}+H_t^{AD}-H_t^{dis}-H_t^{heat}}{c_{AD}\rho_{AD}V_{AD}} \quad \forall t \tag{5}$$

As anaerobic digestion is a temperature-sensitive process, according to the microbial reaction dynamics model proposed in [21], [24], constraints (6) and (7) predict the biogas yield. Given the parameters such as the biochemical methane potential, influent volatile solid concentration, and hydraulic retention time, constraints (6) and (7) essentially reflect the functional relationship between variables $G_t$ and $T_t$. Based on the approximation of nonlinear constraints (6) and (7), we observed that they can be abstracted as a compact form of $G_t=f\left(T_t\right)$ to describe the functional relation between the digesting temperature and the biogas yield. Please note that $\left(T_0,T_1\right)$ and $\left(T_1,T_2\right)$ denote the proper digestion temperature ranges for different digestion types, e.g., mesophilic digestion, thermophilic digestion.

$$\mu_t=\begin{cases}\alpha_{11}\mathrm{e}^{\alpha_{12}T_t} & T_t\in\left(T_0,T_1\right)\\ \alpha_{21}T_t-\alpha_{22} & T_t\in\left(T_1,T_2\right)\end{cases} \tag{6}$$

$$G_t=\frac{B_0S_0V_{AD}}{24\cdot HRT}\left(1-\frac{K}{HRT\cdot\mu_t-1+K}\right) \tag{7}$$

Concerning the non-convexity of constraints (6) and (7), we further piecewisely approximate $G_t=f\left(T_t\right)$ as constraint (8) over the interval $\left[T_0,T_S\right]$, with a set of formulae (9)-(12), where $T_s\in\left(T_0,T_1,...,T_S\right)$.

$$G_t=f\left(T_t\right)\approx\sum_{s=0}^{S}z_{ts}f\left(T_s\right) \quad \forall t \tag{8}$$

$$\begin{cases}T_t=\sum_{s=0}^{S}z_{ts}T_s\\ T_0<T_1<...<T_S\end{cases} \quad \forall t \tag{9}$$

$$\begin{cases}z_{t0}\le q_{t0}\\ z_{ts}\le q_{t(s-1)}+q_{ts} \quad s=1,2...,S-1\\ z_{tS}\le q_{t(S-1)}\end{cases} \tag{10}$$

$$\sum_{s=1}^{S}z_{ts}=1 \quad \forall t \tag{11}$$

$$\sum_{s=0}^{S-1}q_{ts}=1 \quad \forall t \tag{12}$$

In the step of biogas storage, the generated biogas is delivered to the BES and stored for further combustion of the CHP unit. Therefore, the volume of biogas in BES is expressed in (13). Constraints (14) and (15) impose the boundaries on the deflating and inflating rates, respectively. For maintaining continuous daily operation in the next day, the volume of biogas in the BES at the last hour must be no less than the initial volume at the beginning of a day in constraint (16). Please note that the deflating rate of BES is equal to the biogas consumption rate of the CHP unit while the inflating rate of BES is equal to the biogas yield rate of AD, as indicated in Fig. 1. Correspondingly, the total output power of CHP unit is constrained by the biogas consumption rate of CHP unit in constraint (17).

$$G_{t+1}^{BES}=G_t^{BES}+\eta_{BES}G_t-\frac{G_t^{CHP}}{\eta_{BES}} \quad \forall t \tag{13}$$

$$\underline{G}^{BES}\le G_t^{BES}\le\bar{G}^{BES} \quad \forall t \tag{14}$$

$$0\le G_t^{CHP}\le\bar{G}^{CHP} \quad \forall s,\forall t \tag{15}$$

$$G_{24}^{BES}\ge G_0^{BES} \tag{16}$$

$$H_t^{CHP}+P_t^{CHP}=\eta_{con}G_t^{CHP} \quad \forall t \tag{17}$$

In the step of biogas consumption, considering that operation status of the CHP unit should be within its feasible operation region, the heat power and electric power can be represented by a convex combination of the extreme points of the feasible convex region as constraints (18) - (21), where $\left(P_n^{CHP},H_n^{CHP}\right)$ denotes the $n^{\text{th}}$ extreme point of the power-heat feasible operation region of a CHP unit, as shown in Fig. 2. Constraints (22) and (23) impose the boundaries on the thermal and power ramping rates, respectively.

$$P_t^{CHP}=\sum_{n\in SN}y_{tn}P_n^{CHP} \quad \forall t \tag{18}$$

$$H_t^{CHP}=\sum_{n\in SN}y_{tn}H_n^{CHP} \quad \forall t \tag{19}$$

$$\sum_{n\in SN}y_{tn}=m_t \quad \forall t \tag{20}$$

$$0\le y_{tn}\le 1 \quad \forall n\in SN,\forall t \tag{21}$$

$$\left|H_{t+1}^{CHP}-H_t^{CHP}\right|\le H^{\text{ramp}} \quad \forall t \tag{22}$$

$$\left|P_{t+1}^{CHP}-P_t^{CHP}\right|\le P^{\text{ramp}} \quad \forall t \tag{23}$$

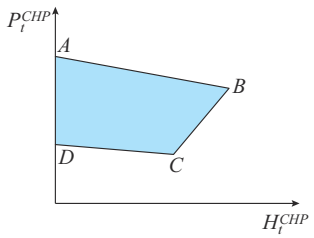


Fig. 2. Power-heat feasible operation region of a CHP unit.

Please note that the above-mentioned expressions (1)-(23) in this section are proposed for illustrating the storage-like characteristic of LBPs in the above-mentioned three steps, which are incorporated as a part of the operational constraints in the upper-level problem in Section III. Also, the subscript of LBP location indicator $g$ is omitted for brevity on the basis that the CHP unit is co-located with the LBP. Through the biogas generation, storage, and consumption, the LBP absorbs the excess power, converts and stores it for later utilization when RESs are no longer available, formulating the time-varying power shifting. With the availability of LBP, the accommodation capacity of the on-site use of RESs will increase and make difference in the local energy market.

## III. Mathematical Formulations of Proposed Bi-level Energy Trading Model

### A. Description of Energy Trading Model

In this subsection, the proposed bi-level energy trading model for the distribution system is illustrated in Fig. 3. The distribution system operator (DSO) is an independent system operator managing the distribution system and runs a centralized dispatch model for keeping the balance of regional load and generation. In a day ahead, the DSO conducts forecasts for load and intermittent sources to formulate a day-ahead procurement and schedule. During the intraday operation, the DSO is responsible for dispatching the power from LBP, DRA, and PV, determining the real-time imported power from the main grid, and keeping the balance of regional load and generation.

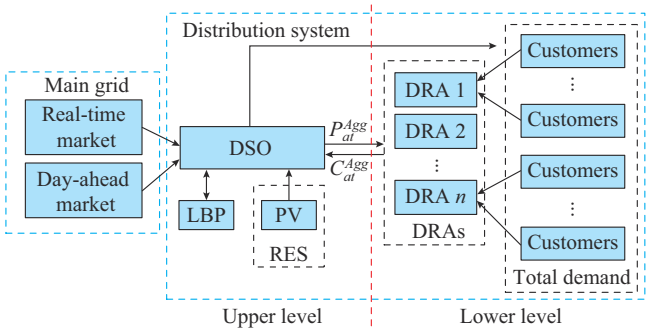


Fig. 3. Description of proposed bi-level energy trading model.

For addressing the influence of LBP on the system dispatch and accommodation of the high penetration of PV, it is noted that the LBP and PV are assumed to be managed by the DSO for keeping the system operation security in this paper. The objective of the upper-level problem is to maximize the social welfare. Thus, the biogas generation, storage, and consumption of LBP and the PV spilling are determined by the DSO in the upper level.

At the demand side in the distribution system, each DRA is a virtual business entity and participates in energy trading independently. It procures the demand reduction of participating consumers with a contractual price for providing balanced power. As a result, the centralized dispatch model forms a bi-level optimization problem, where the DSO maximizes the social welfare subject to the optimal solution in the lower-level problem where the DRA maximizes its profit based on the real-time prices.

The upper-level and lower-level problems are interrelated with the variables of the bidding quantities $P_{at}^{Agg}$ and prices $C_{at}^{Agg}$. Each level has internal and external decision variables that link the upper-level and lower-level problems. The external decision variables of the upper-level problem are the prices for purchasing power $C_{at}^{Agg}$ from DRA and those of the lower-level problem are the bidding quantities $P_{at}^{Agg}$ adjusted by the DRA. For DSO who makes the decision first, the prices of day-ahead markets can also be predicted and can be viewed as known information to the DSO. Therefore, the interactions between DSO, LBP, and DRA can be characterized as the bi-level formulation.

### B. Upper-level Problem: Social Welfare Maximization

The upper-level problem represents the centralized dispatch of DSO to maximize the social welfare, denoted in form of a minimization optimization problem in (24). Constraint (25) denotes that the total benefits of the consumers. Constraints (26), (27), and (28) represent the purchase costs of transactions that took place in the day-ahead market, real-time market, and with DRA, respectively. Constraint (29) depicts the generation/regulation cost of PV and LBP. Constraint (30) is the cost of network losses. It is worth mentioning that to prevent the reverse power flows from feeding back into the main grid and threatening the operation security, exporting power is not allowed in this paper. In other words, $P_{wt}^{RT}$ is a positive variable.

$$\min\left\{-\left(R^{D}-R^{Agg}-R^{DA}-R^{RT}-R^{RES}-R^{loss}\right)\right\} \tag{24}$$

$$R^{D}=\sum_{t}\sum_{k\in SK}C^{D}P_{kt}^{D} \tag{25}$$

$$R^{RT}=\sum_{t}\sum_{w\in SW}C_{t}^{RT}P_{wt}^{RT} \tag{26}$$

$$R^{DA}=\sum_{t}\sum_{w\in SW}C_{t}^{DA}P_{wt}^{DA} \tag{27}$$

$$R^{Agg}=\sum_{t}\sum_{a\in SA}C_{at}^{Agg}P_{at}^{Agg} \tag{28}$$

$$R^{RES}=\sum_{t}\sum_{p\in SP}C^{PV}P_{pt}^{PV}+\sum_{t}\sum_{g\in SG}C^{CHP}P_{gt}^{CHP} \tag{29}$$

$$R^{loss}=\sum_{t}\sum_{i,j\in l\in SL}C_{loss}I_{ijt}R_{ij} \tag{30}$$

The quantity of the purchased power from the day-ahead market is determined according to the historical data of residential load and the forecasted value of PV generation. However, during the intraday operation, the deviation between the forecasted and actual loads cannot be inevitable, thus we use $\varepsilon^{Dem}$ to evaluate the deviation level, as shown by constraints (31)-(33).

$$\sum_{w\in SW}P_{wt}^{DA}+\sum_{p\in SP}\bar{P}_{pt}^{PV}=\sum_{k\in SK}\bar{P}_{kt}^{Dem}\quad\forall t \tag{31}$$

$$\sum_{w\in SW}P_{wt}^{DA}=\sum_{w\in SW}\eta_{PQ}Q_{wt}^{DA}\quad\forall t \tag{32}$$

$$P_{kt}^{Dem}=\varepsilon^{Dem}\bar{P}_{kt}^{Dem}\quad\forall k,\forall t \tag{33}$$

Considering that the profit of DRAs comes from the difference between the revenue of selling demand response reduction and the purchase cost of demand response reduction from the customers, a profit guarantee factor should be set for their profit, as shown in constraint (34).

$$\delta^{Agg}C_{at}^{Aggpro}\le C_{at}^{Agg}\le C_{t}^{RT}\quad\forall a,\forall t \tag{34}$$

At each time step, the power flow at each bus should be balanced. Herein, a convex branch flow model where the active power, reactive power, and bus voltages are taken into consideration is adopted [25]-[27]. Constraints (35) and (36) represent the active and reactive power flow balances at each bus, respectively. Note that the demand at any bus where the LBP is located also includes the active power outflow from the distribution system for electric heating in (37). Constraint (38) calculates the voltage drop along a line.

Constraint (39) adopts a widely-used second-order-cone relaxation methodology to relate the active and reactive power, the voltage magnitude, and the squared current flow magnitude along a line. Constraints (40) and (41) impose the upper and lower limits on nodal voltages and current flows, respectively. Constraints (42)-(44) describe the capacity boundaries of the substation on the real-time balancing power traded with the main grid.

$$\sum_{i\in\Pi_k} P_{ikt} = \sum_{i\in\Pi_k} P_{kjt} - \sum_{p\in\Omega_k} P_{pt}^{PV} - \sum_{w\in\Omega_k}\left(P_{wt}^{RT}+P_{wt}^{DA}\right) - \sum_{g\in\Omega_k}\left(P_{gt}^{CHP}-P_{gt}^{grid}\right) - \left(dr_{kt}-1\right)P_{kt}^{Dem} \quad \forall t,\forall k \tag{35}$$

$$\sum_{i\in\Pi_k} Q_{ikt} = \sum_{i\in\Pi_k} Q_{kjt} - \sum_{w\in\Omega_k}\left(Q_{wt}^{RT}+Q_{wt}^{DA}\right) - \sum_{g\in\Omega_k} Q_{gt}^{CHP} - \left(dr_{kt}-1\right)\eta_{PQ}P_{kt}^{Dem} \quad \forall t,\forall k \tag{36}$$

$$P_{kt}^{D} = P_{kt}^{Dem} + \sum_{g\in\Omega_k} P_{gt}^{grid} \tag{37}$$

$$V_{it} - V_{jt} = 2\left(R_{ij}P_{ijt} + X_{ij}Q_{ijt}\right) - Z_{ij}^2 I_{ijt} \quad \forall i,j\in SK,\forall t \tag{38}$$

$$P_{ijt}^2 + Q_{ijt}^2 \le I_{ijt}V_{it} \quad \forall i,j\in SK,\forall t \tag{39}$$

$$V_i^{\min} \le V_{it} \le V_i^{\max} \quad \forall i\in SK,\forall t \tag{40}$$

$$I_{\min} \le I_{ijt} \le I_{\max} \quad \forall i,j\in SK,\forall t \tag{41}$$

$$Q_{wt}^{RT} + Q_{wt}^{DA} = Q_{wt}^{Sub} \quad \forall t,\forall w \tag{42}$$

$$P_{wt}^{RT} + P_{wt}^{DA} = P_{wt}^{Sub} \quad \forall t,\forall w \tag{43}$$

$$\left(Q_{wt}^{Sub}\right)^2 + \left(P_{wt}^{Sub}\right)^2 \le S_{w,\max}^2 \quad \forall t,\forall w \tag{44}$$

Assuming that the PV spilling is allowed, the actual PV generation is limited by its maximum generation, as shown in constraint (45). The power from the power grid to LBP is limited by the maximum power of the electric heating equipment, as shown in constraint (46).

$$0 \le P_{pt}^{PV} \le \bar{P}_{pt}^{PV} \quad \forall p,\forall t \tag{45}$$

$$0 \le P_{gt}^{grid} \le P_{\max}^{grid} \quad \forall t \tag{46}$$

### C. Lower-level Problem: Profit Maximization of DRAs

In the lower level, the objective is to maximize the profit of each DRA. In (47), the objective of the lower level is represented to minimize the minus-profit of each DRA, consisting of the power purchasing cost from the total regional demand and the minus-profit of selling DRAs' offers to DSO. Constraints (48) and (49) illustrate the active and the reactive power assembled by each DRA, respectively. The boundaries on the aggregated active power and reactive power are constrained in (50) and (51), respectively. Constraint (52) imposes the limits on demand response. $\lambda_{at}^{P}$, $\lambda_{at}^{Q}$, $\bar{\mu}_{at}^{P}$, $\underline{\mu}_{at}^{P}$, $\underline{\mu}_{at}^{Q}$, $\bar{\mu}_{at}^{Q}$, $\underline{v}_{kt}^{dr}$, $\bar{v}_{kt}^{dr}$ are dual variables to (48)-(52), respectively.

$$\min\left\{\sum_t C_{at}^{Aggpro}P_{at}^{Agg} - \sum_t C_{at}^{Agg}P_{at}^{Agg}\right\} \tag{47}$$

$$P_{at}^{Agg} = \sum_{k:(k,a)\in SA} dr_{kt}\cdot P_{kt}^{Dem} \quad \forall t,\forall a:\lambda_{at}^{P} \tag{48}$$

$$Q_{at}^{Agg} = \eta_{PQ}P_{at}^{Agg} \quad \forall t,\forall a:\lambda_{at}^{Q} \tag{49}$$

$$\underline{P}_{at}^{Agg} \le P_{at}^{Agg} \le \bar{P}_{at}^{Agg} \quad \forall t,\forall a:\underline{\mu}_{at}^{P},\bar{\mu}_{at}^{P} \tag{50}$$

$$\underline{Q}_{at}^{Agg} \le Q_{at}^{Agg} \le \bar{Q}_{at}^{Agg} \quad \forall t,\forall a:\underline{\mu}_{at}^{Q},\bar{\mu}_{at}^{Q} \tag{51}$$

$$0 \le dr_{kt} \le dr^{\max} \quad \forall t,\forall k:\underline{v}_{kt}^{dr},\bar{v}_{kt}^{dr} \tag{52}$$

## IV. Solution Method

Though the proposed problem is formulated as a bi-level problem, it still cannot be solved directly. Considering that the lower-level problem is linear and thus convex, this bi-level problem can be solved by representing the low-level problem with the Karush-Kuhn-Tucker (KKT) conditions, which are widely adopted [28] - [30]. By using the KKT theorem, the KKT conditions of the lower-level problem can be derived as (53)-(61).

$$C_{at}^{Aggpro} - C_{at}^{Agg} + \lambda_{at}^{P} - \eta_{PQ}\lambda_{at}^{Q} - \underline{\mu}_{at}^{P} + \bar{\mu}_{at}^{P} = 0 \quad \forall a,\forall t \tag{53}$$

$$\lambda_{at}^{Q} - \underline{\mu}_{at}^{Q} + \bar{\mu}_{at}^{Q} = 0 \quad \forall a,\forall t \tag{54}$$

$$-\lambda_{at}^{P}P_{kt}^{Dem} - \underline{v}_{kt}^{dr} + \bar{v}_{kt}^{dr} = 0 \quad \forall k:(k,a)\in SA,\forall t \tag{55}$$

$$0 \le \left(P_{at}^{Agg} - \underline{P}_{at}^{Agg}\right) \perp \underline{\mu}_{at}^{P} \ge 0 \quad \forall a,\forall t \tag{56}$$

$$0 \le \left(\bar{P}_{at}^{Agg} - P_{at}^{Agg}\right) \perp \bar{\mu}_{at}^{P} \ge 0 \quad \forall a,\forall t \tag{57}$$

$$0 \le \left(Q_{at}^{Agg} - \underline{Q}_{at}^{Agg}\right) \perp \underline{\mu}_{at}^{Q} \ge 0 \quad \forall a,\forall t \tag{58}$$

$$0 \le \left(\bar{Q}_{at}^{Agg} - Q_{at}^{Agg}\right) \perp \bar{\mu}_{at}^{Q} \ge 0 \quad \forall a,\forall t \tag{59}$$

$$0 \le \left(dr_{kt}^{\max} - dr_{kt}\right) \perp \bar{v}_{kt}^{dr} \ge 0 \quad \forall k,\forall t \tag{60}$$

$$0 \le dr_{kt} \perp \underline{v}_{kt}^{dr} \ge 0 \quad \forall k,\forall t \tag{61}$$

However, the complementarity constraints (56) - (61) are nonlinear and nonconvex caused by the product of two variables, and cannot be directly solved by the commercial solver. Herein, the widely-adopted big-$M$ relaxation is used for linearizing $x \perp y$ in constraints (56)-(61). A compact form of the big-$M$ relaxation is proposed in (62) and (63), where $M$ is a sufficiently big number and $z$ is a binary variable.

$$0 \le x \le Mz \tag{62}$$

$$0 \le y \le M(1-z) \tag{63}$$

After the transformation of the lower-level problem, the upper-level optimization objective is still a nonlinear problem due to the product of variables $C_{at}^{Agg}$ and $P_{at}^{Agg}$ in (29). It can be equivalently replaced by (64) based on the strong duality theorem that a feasible solution of the primal and dual problems is obtained given that if and only if primal and dual objective functions are equal. Substituting the results in (64) into the objective function (29), (29) can be derived into (65).

$$\sum_t C_{at}^{Aggpro}P_{at}^{Agg} - \sum_t C_{at}^{Agg}P_{at}^{Agg} = -\sum_t \sum_{k:(k,a)\in SA} \bar{v}_{kt}^{dr}dr^{\max} - \sum_t\left(\bar{P}_{at}^{Agg}\bar{\mu}_{at}^{P} - \underline{P}_{at}^{Agg}\underline{\mu}_{at}^{P} - \underline{\mu}_{at}^{Q}\underline{Q}_{at}^{Agg} + \bar{Q}_{at}^{Agg}\bar{\mu}_{at}^{Q}\right) \quad \forall a \tag{64}$$

$$R^{Agg}=\sum_a\sum_t C_{at}^{Aggpro}P_{at}^{Agg}+\sum_a\sum_t\sum_{k(k,a)\in SA}\bar{v}_{kt}^{dr}dr^{\max}+\sum_a\sum_t\left(\bar{P}_{at}^{Agg}\bar{\mu}_{at}^{P}-\underline{P}_{at}^{Agg}\underline{\mu}_{at}^{P}-\underline{\mu}_{at}^{Q}\underline{Q}_{at}^{Agg}+\bar{Q}_{at}^{Agg}\bar{\mu}_{at}^{Q}\right) \quad (65)$$

In this way, this bi-level problem is transformed into a single-level mixed-integer second-order-cone mathematical program with equilibrium constraint (MPEC) problem, which incorporates its primal constraints of the lower-level problem and its dual strong condition constraints into the upper level as:

$$\begin{cases}\min\left\{-\left(R^{D}-R^{Agg}-R^{DA}-R^{RT}-R^{RES}-R^{loss}\right)\right\}\\ \text{s.t. (1)-(5), (8)-(23), (25)-(46), (48)-(55), (62)-(65)}\end{cases} \quad (66)$$

## V. Case Studies

The proposed model is formulated using a deterministic method for calculating its accommodation capacity of RES with a given PV penetration level. It is developed in GAMS and solved by the Cplex solver. All tests are carried out on a PC with an Intel Core i7 CPU at 3.40 GHz and 4 GB of RAM. The topology of a modified IEEE 33-bus distribution system owned and operated by a DSO is presented in Fig. 4 [31].

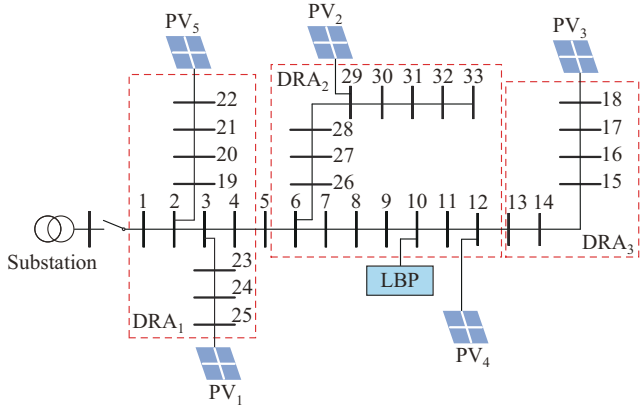


Fig. 4. Topology of modified IEEE 33-bus distribution system.

The capacity of the substation is 3 MVA. The voltage at the reference bus (substation bus) is 24.9 kV. The price of importing power in the real-time market and the contractual prices with DRA are cited from [32], where the peak-price periods appear at 10:00-13:00 and 18:00-21:00. The profit guarantee factor held by each DRA is identical and equal to 1.1. The load price at each bus is 0.12 \$/kW. Given that the AD is cylindrical with an identical height and radius of 12 m, the volume of AD is 5425 $m^3$ with a surface area of 1808 $m^2$. The maximum power output of the CHP unit is 400 kW while the maximum power from the power grid to AD is 600 kW. The power factor of the CHP unit is 0.85 lagging. In the anaerobic digestion process, $S_0$ is 60 g/kg, $B_0$ is 0.343 $m^3$/kg, and *HRT* is 25 days. The extreme points $\left(P_n^{CHP}, H_n^{CHP}\right)$ of the feasible convex region are $A$(400, 0), $D$(200, 0), $C$(150, 100), $B$(300, 250) and the ramping rate that reflects the power difference between time steps is 150 kW/h. The digesting temperature is set at around 25 °C. The heat transfer coefficient is 0.005 kW/($m^2$·°C).

PV penetration levels from 30% to 50% with 10% increments are studied, where the PV penetration level is defined as the ratio of daily PV generation to the total daily demand. The generation of each PV farm takes up 10% of the total daily regional demand. Instead, for each 10% penetration increment, one PV farm is added sequentially, for example, when at 40% penetration level, PV farms $PV_1$, $PV_2$, $PV_3$, $PV_4$ are installed in this region. As these PV farms are located close to each other because of the limited coverage of the distribution system, their hourly generations are similar in view of their identical capacity.

The expected PV generation at different PV penetration levels and the total demand are shown in Fig. 5. It can be observed from Fig. 5 that even when the PV penetration level is at 30%, the PV generation exceeds the total demand during 10:00-16:00. During this period, DSO has to make decisions to curtail PV generation to maintain the power balance if no load shifting or energy storage exists. To illustrate the impact of the storage-like characteristics of LBPs on the system dispatch and economic performance, we demonstrate two following cases. The computation time of Cases 1 and 2 at any PV penetration level is all below 30 s.

1) Case 1: the proposed model incorporating both LBP and DRA.

2) Case 2: the proposed model incorporating the DRA alone.

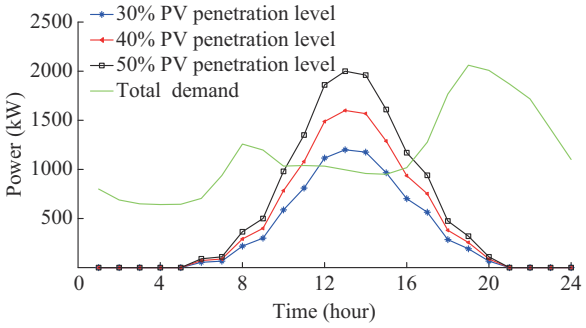


Fig. 5. Expected PV generation at different PV penetration levels and total demand.

### A. Impact of LBP on System Dispatch and Economic Performance

Limited by the prohibition of the reverse flow to the main grid via substation, the distribution system has a limited capacity to accommodate large amount of PV generation. Thus, the actual PV generation dispatched in the system must be less than the expected PV generation, given that the PV curtailment is allowed. Herein, a utilization rate (UR) is defined as the ratio of the actual PV generation to the expected PV generation.

Figure 6 shows the hourly UR of Cases 1 and 2 at different PV penetration levels with the load forecasting multiplier $\varepsilon^{Dem}=1.1$. It can be observed that the hourly UR of Case 1 is much higher than that of Case 2 during the period when the PV generation is sufficient. Without the LBP, the expected PV generation that exceeds the total demand in Fig. 5 is curtailed, and the corresponding hourly UR is shown in Fig. 6(b). Comparing Fig. 6(a) with Fig. 6(b), it can be found

that the hourly UR is obviously higher in Case 1 than that in Case 2 during 11: 00-17: 00, which illustrates that the LBP contributes to the better accommodation of PV generation. The total UR of the two cases at different PV penetration levels is further summarized in Table I.

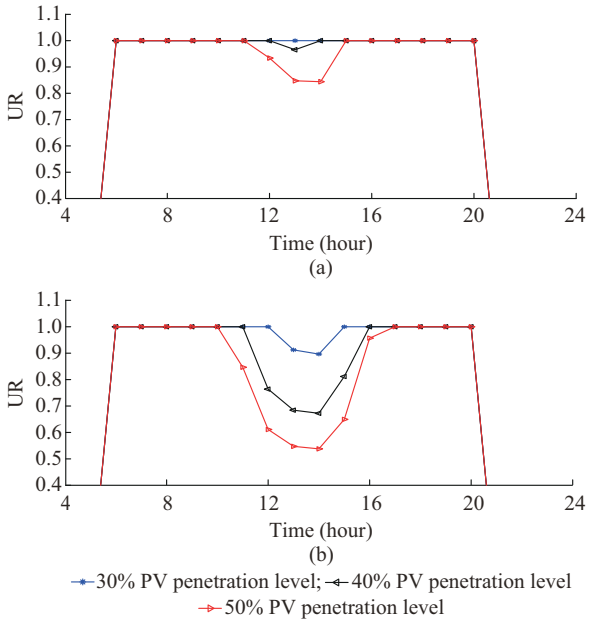


Fig. 6. Hourly UR of Cases 1 and 2 at different PV penetration levels. (a) Case 1. (b) Case 2.

TABLE I
TOTAL UR OF CASES 1 AND 2 AT DIFFERENT PV PENETRATION LEVELS

| PV penetration level (%) | Total UR (%) | |
|---|---|---|
| | Case 1 | Case 2 |
| 30 | 100.0 | 93.7 |
| 40 | 99.5 | 81.4 |
| 50 | 94.7 | 75.8 |

To further illustrate the reason of different total URs in Cases 1 and 2 in Table I and Fig. 6, the hourly dispatch results of the heat and electric power of the CHP unit, the power from the distribution system to the LBP, and the volume of biogas in the BES at different PV penetration levels in Case 1 are presented in Fig. 7. It can be observed that the power from the distribution system to the LBP increases with the PV penetration level. This is because a more sufficient energy supply is provided by the PV generation, with the prohibition of reverse flow to the main grid, as indicated in Fig. 7(a) and (b). It can be also observed that, except for some periods, the power from the distribution system to the LBP is the largest for maintaining the digesting temperature over the daily horizon. Taking Fig. 7(a) as an example, during the periods 10:00-13:00 and 18:00-21:00, the total generation of PV, CHP unit, and DRA cannot cover the total demand after the demand response, and it is too expensive to import power from the real-time market during the peak-price period. For maximizing the social welfare, the DSO chooses to reduce the power to LBP but to meet the total demand of customers as its primary goal.

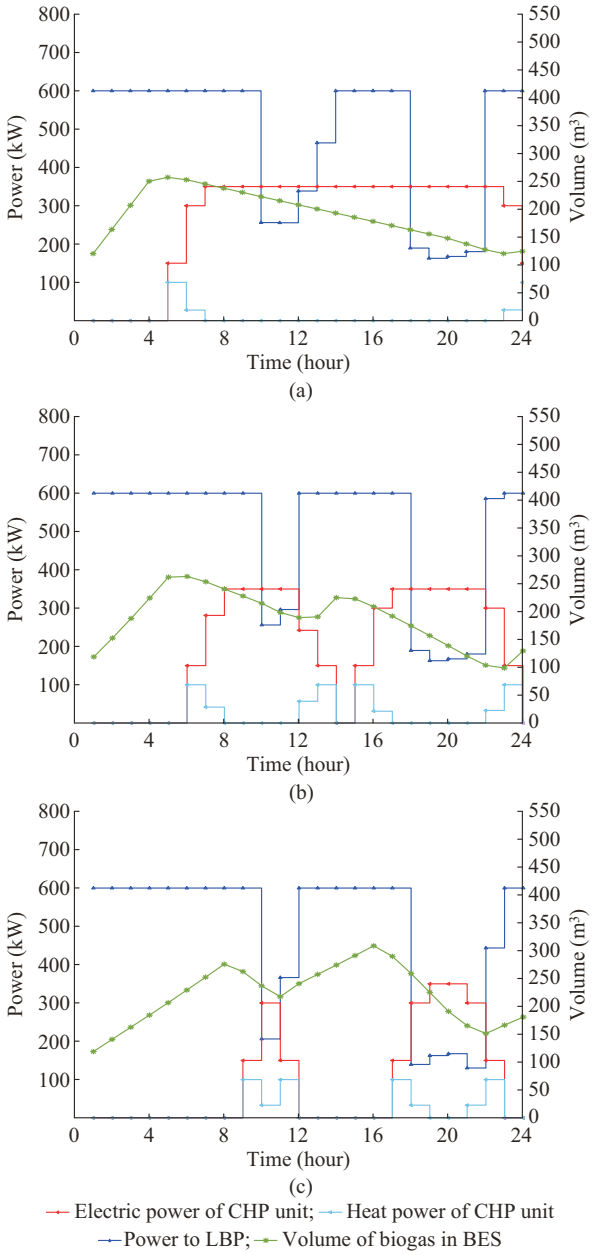


Fig. 7. Hourly dispatch results at different PV penetration levels in Case 1. (a) 30% PV penetration level. (b) 40% PV penetration level. (c) 50% PV penetration level.

It is worth mentioning that according to the results in Table I, the total UR in Case 1 does not decrease proportionally with the increase of PV penetration level. Comparing Fig. 7(b) and (c), it can be observed that the power from the distribution system to LBP is similar to each other, indicating that the LBP has already reached the maximum accommodation capacity when operating at 40% PV penetration level. This finally causes an obvious drop of UR from 99.5% to 94.7% in Table I. Meanwhile, it can be observed from Fig. 7 that the electric power of CHP unit lowers down as the PV penetration level increases in the daytime. This is because the increasing PV generation will compress the electric power share of the CHP unit as the total demand is fixed. Opposed to the obvious variation of electric power generated

by the CHP unit in Fig. 7(a), (b), and (c), the heat power generated by the CHP unit keeps similar. Besides, it is also confusing about the decision of the LBP on generating heat power for AD to produce and store more biogas, which formulates an inefficient process from discharging energy to storing energy. From the feasible operation region of the CHP unit, it can be observed that the extreme points $\left(P_n^{CHP}, H_n^{CHP}\right)$ of the feasible convex region are $A(400, 0)$, $D(200, 0)$, $C(150, 100)$, $B(300, 250)$, while the ramping rate that reflects the power difference between time steps is 150 kW/h. It indicates that the CHP unit must go through a period of generating heat power and electric power simultaneously before starting up or shutting down. This also explains why the profile of heat power of the CHP unit seems to be symmetrical along the time horizon.

Regarding to the system dispatch of the DSO, Fig. 8 shows the results of output power of PV, the power purchased from DRA, and the power purchased from the real-time and day-ahead markets at 40% PV penetration level. Obviously, it can be observed that the power purchased from DRA is very limited in both cases because of the limitation of the demand response capacity and physical boundaries. One major difference between the two cases is the output power profile of PV, and the other is that the power purchased from the real-time market is much higher in Case 1, especially when both the electricity price and the customers' demand are relatively low. During the low-price period, the low-price power is purchased by the DSO to feed into the LBP to produce more biogas as the backup fuel to supply the electric power when the PV is not available, which also causes a rise of $R^{RT}$ in Case 1 in Table II.

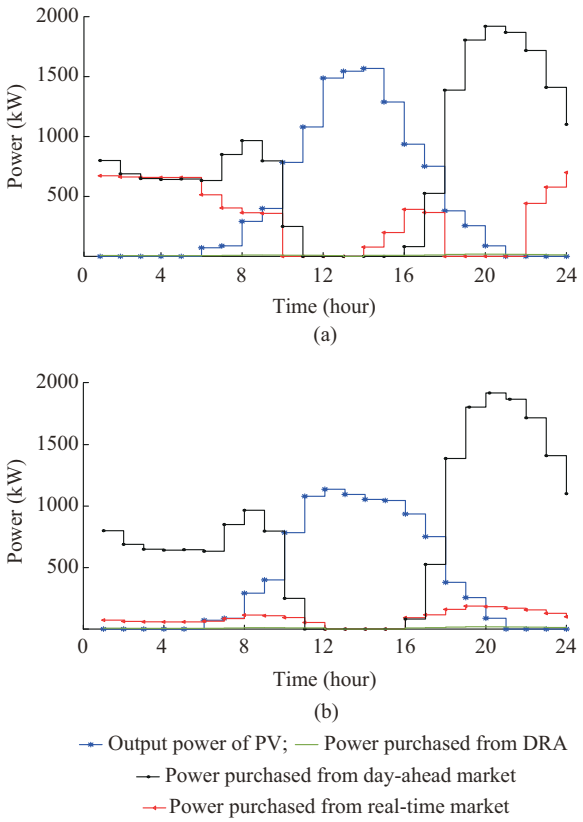


Fig. 8. Hourly dispatch results of DSO at 40% PV penetration level in Cases 1 and 2. (a) Case 1. (b) Case 2.

TABLE II
ECONOMIC PERFORMANCE AT DIFFERENT PV PENETRATION LEVELS

| $\varepsilon^{Dem}$ | Case | PV penetration level (%) | $R^{loss}$ ($) | Profit of DRA ($) | $R^{Agg}$ ($) | $R^{RES}$ ($) | $R^{RT}$ ($) | $R^{D}$ ($) | Social welfare ($) |
|---|---|---|---|---|---|---|---|---|---|
| 1.0 | 1 | 30 | 119 | 13 | 11.0 | 556 | 267 | 4867 | 2481 |
| | | 40 | 135 | 11 | 9.0 | 561 | 322 | 4889 | 2539 |
| | | 50 | 153 | 10 | 9.0 | 475 | 412 | 4886 | 2586 |
| | 2 | 30 | 59 | 0 | 0.0 | 155 | 0 | 3332 | 1685 |
| | | 40 | 65 | 0 | 0.0 | 180 | 0 | 3332 | 1763 |
| | | 50 | 64 | 0 | 0.0 | 198 | 0 | 3332 | 1819 |
| 1.1 | 1 | 30 | 126 | 13 | 11.0 | 556 | 369 | 5058 | 2564 |
| | | 40 | 139 | 12 | 10.0 | 610 | 549 | 5110 | 2629 |
| | | 50 | 160 | 11 | 9.0 | 482 | 487 | 5082 | 2692 |
| | 2 | 30 | 64 | 10 | 12.0 | 162 | 159 | 3664 | 1795 |
| | | 40 | 78 | 11 | 26.0 | 189 | 188 | 3664 | 1878 |
| | | 50 | 77 | 10 | 7.9 | 210 | 173 | 3664 | 1946 |

A detailed economic comparison for two cases at different PV penetration levels is presented in Table II, where the results are divided into two groups. One group is calculated with no load forecasting multiplier ($\varepsilon^{Dem} = 1.0$), and the other is with 10% multiplier ($\varepsilon^{Dem} = 1.1$). It can be observed that when $\varepsilon^{Dem} = 1.0$, the DRA does not have to provide flexibility in Case 2, thus, the profit of DRA, as well as the aggregated power, is equal to zero. Accordingly, no power is imported as $R^{RT} = 0$.

While in Case 1, the LBP stores the surplus electricity and shifts the load, which results in the increase of the social welfare and the profit of DRA. In contrast, when $\varepsilon^{Dem} = 1.1$, both the social welfare and the profit of DRA in Case 1 are higher than those in Case 2. Besides, due to the implementation of the LBP, the cost for purchasing power from the main grid in Case 1 is higher than that in Case 2, which is because the DSO can make flexible decisions on whether to purchase power from the main grid or LBP considering the real-time price.

### B. Sensitivity Analysis

To fully evaluate the storage-like characteristic of LBPs contributing to accommodating RESs, a sensitivity analysis is conducted.

#### 1) Sensitivity Analysis on $P_{\max}^{grid}$

In Fig. 7, it is observed that the surplus PV generation in the daytime is primarily injected into the LBP by $P_{gt}^{grid}$ who is limited by $P_{\max}^{grid}$. Therefore, the parameter variation of $P_{gt}^{grid}$ may influence the optimization results. In the analysis, the value of $P_{\max}^{grid}$ is within [360 kW, 840 kW] with a step of 120 kW. It can be observed from Fig. 9 that the increase of $P_{\max}^{grid}$ has a large influence on improving the accommodation capacity of LBPs, where both the social welfare and the total UR increase with $P_{\max}^{grid}$. However, though a high-power electric heating device embedded inside the digester can help accommodate the RES better, its rated heating power is also determined by the heating requirement of the sizes and types of the AD. An improper electric heating power may cause instability and even failure in the anaerobic digestion process.

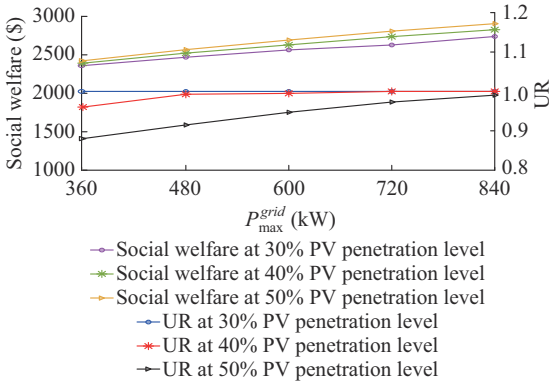


Fig. 9. Sensitivity analysis on $P_{\max}^{grid}$.

#### 2) Sensitivity Analysis on the Maximum Power Output of CHP Unit

In Fig. 7, the electricity supply is compensated by the maximum power output of the CHP unit when the PV generation is insufficient. Thus, the sensitivity analysis on the maximum power output of the CHP unit should be conducted as well. In the analysis, the maximum power output of CHP unit varies from 300 kW to 700 kW. However, as observed from Fig. 10, the maximum power output does not has a direct influence on the accommodation capacity of LBPs. This is because the output power of CHP unit is mainly used as a backup to supply electricity during the peak-load period. Therefore, it is observed that only the UR slightly increases with the maximum power output of CHP unit.

#### 3) Sensitivity Analysis on Demand Response Capacity

Considering that the demand response capacity can influence the quantity of the demand reduction as well as the optimization results, a sensitivity analysis on the demand response capacity is conducted. To stimulate the flexibility of DRA, the load forecasting multiplier is set at $\varepsilon^{Dem}=1.05$, which indicates that the relative deviation between the actual and predictive active loads is 5%. Assuming that $dr^{\max}$ ranges from 0.05 to 0.25 with a step of 0.05, when the relative deviation between the actual and predictive active loads is lower than $dr^{\max}$, the maximum accommodation capacity of PV cannot be easily reached with the flexibility provided by the DRA alone in Fig. 11. However, when the value of $dr^{\max}$ is higher than the relative deviation between the actual and predictive active loads, the total demand can be easily satisfied and there is no more space for the DRA to offer its flexibility, which finally has no influence on the total UR and social welfare.

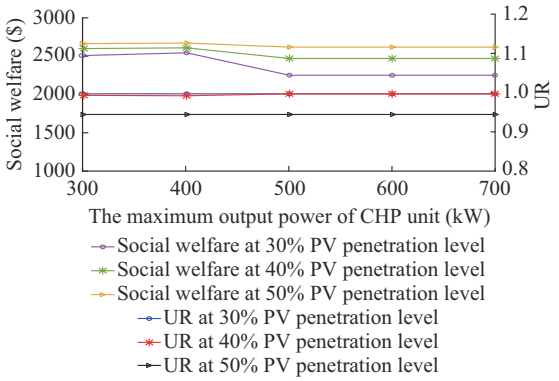


Fig. 10. Sensitivity analysis on the maximum power output of CHP unit.

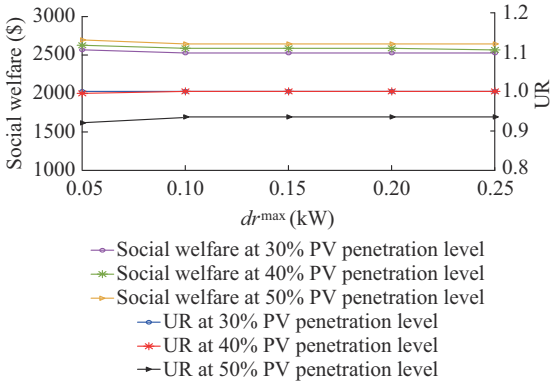


Fig. 11. Sensitivity analysis on $dr^{\max}$.

#### 4) Sensitivity Analysis on Load Forecasting Error

Because the quantity of the purchasing power in the day-ahead market is decided by the prediction of PV generation and the total demand according to constraints (31)-(33), any variation of the total demand will influence the regional power balance, the imported power as well as the optimization results in the intraday operation. Herein, the prediction error of the total demand is analogized by imposing the load forecasting multiplier $\varepsilon^{Dem}$ with a range of [0.9, 1.2]. When the PV penetration level is 30%, as observed from Fig. 12, the social welfare grows faster after $\varepsilon^{Dem}$ reaches 1.0. The total UR at any penetration level does not increase until it reaches 100%. This is because that when $\varepsilon^{Dem}$ is between 0.9 and 1.0, the actual total demand is less than the forecasted value, and the requirement for balancing power is high. In contrast, when $\varepsilon^{Dem}$ is between 1.0 and 1.2, the actual total demand exceeds the power purchased from the day-ahead market, and the LBP contributes to storing and shifting the surplus PV generation to compensate for the electricity supply, which causes an increase of the total UR and the social welfare.

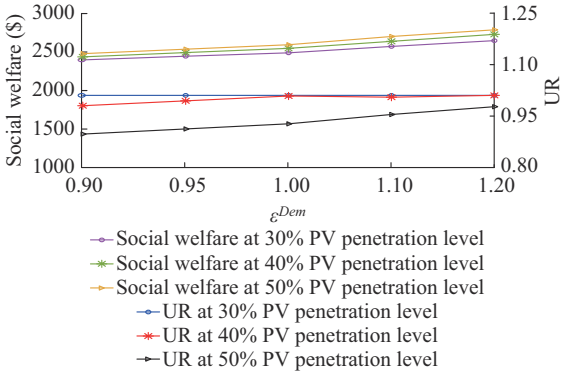


Fig. 12. Sensitivity analysis on $\varepsilon^{Dem}$.

## VI. Conclusion

With the increasing penetration of RESs, this paper utilizes the storage-like characteristic of LBPs to help better accommodate the local RESs in the rural areas via a bi-level trading energy market that incorporates the LBP and DRA. The main findings in this paper are summarized as follows.

1) The storage-like characteristic of LBPs is discovered with a detailed model of the conversion process of power-biogas-power consisting of biogas generation, storage, and consumption.

2) A bi-level energy trading model is proposed for maximizing the social welfare and the profit of DRAs while quantifying the accommodation capacity contributed by the LBP. The results show that the proposed model incorporating LBP has better economic performance and improves the accommodation capacity of the on-site use of PV up to 6.3%, 18.1%, and 18.9% at 30%, 40%, and 50% PV penetration levels, respectively.

3) A detailed sensitivity analysis of the maximum power from the distribution system to the LBP, the maximum power output of CHP unit, the demand response capacity, and the load forecasting error is conducted, where the maximum power from the distribution system to the LBP influences the accommodation capacity most.

Considering the analogous characteristics of the LBP with ESS, our future work will move towards the auxiliary market supported by the LBP, e.g., flexibility and reserve markets, to explore various local energy markets to help better accommodate RESs and make the LBP profitable.

## References

[1] B. Stürmer, F. Theuretzbacher, and E. Saracevic, "Opportunities for the integration of existing biogas plants into the Austrian electricity market," *Renewable and Sustainable Energy Reviews*, vol. 138, p. 110548, Mar. 2020.

[2] L. Tian, L. Cheng, J. Guo *et al*., "System modeling and optimal dispatching of multi-energy microgrid with energy storage," *Journal of Modern Power Systems and Clean Energy*, vol. 8, no. 5, pp. 809-819, Sept. 2020.

[3] D. Fooladivanda, C. Rosenberg, and S. Garg, "Energy storage and regulation: an analysis," *IEEE Transactions on Smart Grid*, vol. 7, no. 4, pp. 1813-1823, Jul. 2016.

[4] A. G. Olabi, C. Onumaegbu, T. Wilberforce *et al*., "Critical review of energy storage systems," *Energy*, vol. 214, p. 118987, Jan. 2021.

[5] N. Li and K. W. Hedman, "Economic assessment of energy storage in systems with high levels of renewable resources," *IEEE Transactions on Sustainable Energy*, vol. 6, no. 3, pp. 1103-1111, Jul. 2015.

[6] H. Alharbi and K. Bhattacharya, "Participation of pumped hydro storage in energy and performance-based regulation markets," *IEEE Transactions on Power Systems*, vol. 35, no. 6, pp. 4307-4323, Nov. 2020.

[7] M. Chazarra, J. I. Perez-Diaz, and J. Garcia-Gonzalez, "Optimal joint energy and secondary regulation reserve hourly scheduling of variable speed pumped storage hydropower plants," *IEEE Transactions on Power Systems*, vol. 33, no. 1, pp. 103-115, Jan. 2018.

[8] M. A. Hozouri, A. A. Baspour, M. Fotuhi-Firuzabad *et al*., "On the use of pumped storage for wind energy maximization in transmission-constrained power systems," *IEEE Transactions on Power Systems*, vol. 30, no. 2, pp. 1017-1025, Nov. 2014.

[9] W. F. Pickard, "The history, present state, and future prospects of underground pumped hydro for massive energy storage," *Proceedings of the IEEE*, vol. 7, pp. 473-483, Jul. 2011.

[10] L. Tziovani, L. Hadjidemetriou, C. Charalampous *et al*., "Energy management and control of a flywheel storage system for peak shaving applications," *IEEE Transactions on Smart Grid*, vol. 12, no. 5, pp. 4195-4207, Sept. 2021.

[11] R. Khatami, K. Oikonomou, and M. Parvania, "Look-ahead optimal participation of compressed air energy storage in day-ahead and real-time markets," *IEEE Transactions on Sustainable Energy*, vol. 11, no. 2, pp. 682-692, Apr. 2020.

[12] S. Shafiee, H. Zareipour, A. M. Knight *et al*., "Risk-constrained bidding and offering strategy for a merchant compressed air energy storage plant," *IEEE Transactions on Power Systems*, vol. 32, no. 2, pp. 946-957, Mar. 2017.

[13] G. Pan, W. Gu, Y. Lu *et al*., "Accurate modeling of a profit-driven power to hydrogen and methane plant toward strategic bidding within multi-type markets," *IEEE Transactions on Smart Grid*, vol. 12, no. 1, pp. 338-349, Jan. 2021.

[14] Q. Huang, Y. Xu, and C. Courcoubetis, "Financial incentives for joint storage planning and operation in energy and regulation markets," *IEEE Transactions on Power Systems*, vol. 34, no. 5, pp. 3326-3339, Sept. 2019.

[15] B. Wang, C. Zhang, and Z. Y. Dong, "Interval optimization-based coordination of demand response and battery energy storage system considering SOC management in a microgrid," *IEEE Transactions on Sustainable Energy*, vol. 11, no. 4, pp. 2922-2931, Oct. 2020.

[16] A. Nikoobakht, J. Aghaei, M. Shafie-Khah *et al*., "Assessing increased flexibility of energy storage and demand response to accommodate a high penetration of renewable energy sources," *IEEE Transactions on Sustainable Energy*, vol. 10, no. 2, pp. 659-669, Apr. 2019.

[17] R. O'Shea, D. M. Wall, and J. D. Murphy, "An energy and greenhouse gas comparison of centralised biogas production with road haulage of pig slurry, and decentralised biogas production with biogas transportation in a low-pressure pipe network," *Applied Energy*, vol. 208, pp. 108-122. Dec. 2017.

[18] T. Luo, J. Pan, L. Fu *et al*., "Reducing biogas emissions from village-scale plant with optimal floating-drum biogas storage tank and operation parameters," *Applied Energy*, vol. 208, pp. 312-318, Dec. 2017.

[19] L. Jürgensen, E. A. Ehimen, J. Born *et al*., "Utilization of surplus electricity from wind power for dynamic biogas upgrading: northern Germany case study," *Biomass Bioenergy*, vol. 66, pp. 126-132, Jul. 2014.

[20] E. S. Gaballah, T. K. Abdelkader, S. Luo *et al*., "Enhancement of biogas production by integrated solar heating system: a pilot study using tubular digester," *Energy*, vol. 193, p. 116758, Feb. 2020.

[21] B. Su, H. Wang, X. Zhang *et al*., "Using photovoltaic thermal technology to enhance biomethane generation via biogas upgrading in anaerobic digestion," *Energy Conversion and Management*, vol. 235, p. 113965, May 2021.

[22] A. Nazari, M. Soltani, M. Hosseinpour *et al*., "Integrated anaerobic co-digestion of municipal organic waste to biogas using geothermal and CHP plants: a comprehensive analysis," *Renewable and Sustainable Energy Reviews*, vol. 152, p. 111709, Dec. 2021.

[23] C. Li, H. Yang, M. Shahidehpour *et al*., "Optimal planning of islanded integrated energy system with solar-biogas energy supply," *IEEE Transactions on Sustainable Energy*, vol. 11, no. 4, pp. 2437-2448, Oct. 2020.

[24] Y. R. Chen and A. G. Hashimoto, "Kinetics of methane fermentation," *Biotechnology and Bioengineering Symposium*, vol. 8, no. 11, pp. 503-511, Jan. 1978.

[25] M. Farivar and S. H. Low, "Branch flow model: relaxations and convexification—Part I," *IEEE Transactions on Power Systems*, vol. 28, no. 3, pp. 2554-2564, Aug. 2013.

[26] N. Li, L. Chen, and S. H. Low, "Exact convex relaxation of OPF for radial networks using branch flow model," in *Proceedings of 2012 IEEE Third International Conference on Smart Grid Communications*

*(SmartGridComm)*, Tainan, China, Nov. 2012, pp. 7-12.
[27] R. Zhang, T. Jiang, F. Li *et al*., "Conic optimal energy flow of integrated electricity and natural gas systems," *Journal of Modern Power Systems and Clean Energy*, vol. 9, no. 4, pp. 963-967, Jul. 2021.
[28] J. Kazempour and B. F. Hobbs, "Value of flexible resources, virtual bidding, and self-scheduling in two-settlement electricity markets with wind generation—Part I: principles and competitive model," *IEEE Transactions on Power Systems*, vol. 33, no. 1, pp. 749-759, Jan. 2018.
[29] H. Guo, Q. Chen, X. Fang *et al*., "Efficiency loss for variable renewable energy incurred by competition in electricity markets," *IEEE Transactions on Sustainable Energy*, vol. 11, no. 3, pp. 1951-1964, Jul. 2020.
[30] S. Mousavian, B. Raouf, and A. J. Conejo, "Equilibria in interdependent natural-gas and electric power markets: an analytical approach," *Journal of Modern Power Systems and Clean Energy*, vol. 9, no. 4, pp. 776-787, Jul. 2021.
[31] H. Wang, Z. Yan, M. Shahidehpour *et al*., "Quantitative evaluations of uncertainties in multivariate operations of microgrids," *IEEE Transactions on Smart Grid*, vol. 11, no. 4, pp. 2892-2903, Jul. 2020.
[32] C. Zhang, Q. Wang, J. Wang *et al*., "Real-time procurement strategies of a proactive distribution company with aggregator-based demand response," *IEEE Transactions on Smart Grid*, vol. 9, no. 2, pp. 766-776, Mar. 2018.

**Hanyu Yang** received the B.E. and the Ph.D. degrees from the College of Electrical Engineering, Hunan University, Changsha, China, in 2015 and 2021, respectively. She is currently a Lecturer with College of Electrical Engineering and Control Science, Nanjing Tech University, Nanjing, China. She was a Visiting Scholar at Robert W. Galvin Center for Electricity Innovation at Illinois Institute of Technology, Chicago, USA. Her research interests include power system planning and integrated energy system.

**Canbing Li** received the B.E. and Ph.D. degrees from Tsinghua University, Beijing, China, in 2001 and 2006, respectively, both in electrical engineering. He is currently a Professor with the School of Electronic Information and Electrical Engineering, Shanghai Jiao Tong University, Shanghai, China. His research interests include power systems, smart grid, renewable energy, with an emphasis on large-scale power system dispatch, economic and secure operation of power systems, energy efficiency and energy saving in smart grid, electric demand management of data centers, and vehicle-to-grid technologies.

**Ruanming Huang** received the M.S. degree from the School of Electrical Engineering, Southeast University, Nanjing, China, in 2007. He is currently working with Economic and Technological Research Institute of Shanghai Electric Power Company, Shanghai, China. His research interests include power system planning and renewable energy integration.

**Feng Wang** received the B.E. degree from the School of Electrical Engineering and Automation, Henan Polytechnic University, Jiaozuo, China, in 2019. Currently, he is pursuing the M.S. degree in electrical engineering with the College of Electrical and Information Engineering, Hunan University, Changsha, China. His research interests include electricity-hydrogen energy system optimization and operation.

**Lili Hao** received the B.S. and M.S. degrees from Hohai University, Nanjing, China, in 2001 and 2004, respectively, and the Ph.D. degree from Southeast University, Nanjing, China, in 2010. She was a Visiting Scholar in the School of Electrical Engineering and Computer Science, Washington State University, Pullman, USA, from 2015 to 2016. She is currently an Assistant Professor at Nanjing Tech University, Nanjing, China. Her research interests include power system security and reliability.

**Qiuwei Wu** received the Ph.D. degree in power system engineering from Nanyang Technological University, Singapore, in 2009. He worked at Department of Electrical Engineering, Technical University of Denmark (DTU), Copenhagen, Denmark, since 2009. He is currently with Tsinghua-Berkeley Shenzhen Institute, Tsinghua Shenzhen International Graduate School, Tsinghua University, Shenzhen, China. His research interests include operation and control of power systems with high penetration of renewables, including wind power modelling and control, active distribution networks, and operation of integrated energy systems.

**Long Zhou** received the B.E. degree in Shanghai University of Electric Power, Shanghai, China, in 2006, and the Ph.D. degree from School of Engineering and Mathematical Science, City University of London, London, UK, in 2010. He is currently a General Manager Assistant at the Information Center of Guangdong Power Grid Company Limited, Guangzhou, China. His research interests include smart grid, power quality, and big data technology.